Atomic diffusion across $Ni_{50}Ti_{50}$–Cu explosive welding interface: Diffusion layer thickness and atomic concentration distribution*

Chen Shi-Yang(陈仕洋)[a], Wu Zhen-Wei(武振伟)[a], and Liu Kai-Xin(刘凯欣)[a)b)†]

[a)] *LTCS and Department of Mechanics and Engineering Science, College of Engineering, Peking University, Beijing* 100871, *China*
[b)] *Center for Applied Physics and Technology, Peking University, Beijing* 100871, *China*

(Received 7 October 2013; revised manuscript received 11 December 2013; published online 10 April 2014)

Molecular dynamics simulations are carried out to study atomic diffusion in the explosive welding process of $Ni_{50}Ti_{50}$–Cu (at.%). By using a hybrid method which combines molecular dynamics simulation and classical diffusion theory, the thickness of the diffusion layer and the atomic concentration distribution across the welding interface are obtained. The results indicate that the concentration distribution curves at different times have a geometric similarity. According to the geometric similarity, the atomic concentration distribution at any time in explosive welding can be calculated. $Ni_{50}Ti_{50}$–Cu explosive welding and scanning electron microscope experiments are done to verify the results. The simulation results and the experimental results are in good agreement.

Keywords: diffusion, interfaces, explosive welding, molecular dynamics

PACS: 68.35.Fx, 02.70.Ns **DOI:** 10.1088/1674-1056/23/6/066802

1. Introduction

Explosive welding is a solid state welding process, which uses a controlled explosive detonation to force two metals together at high pressure. It enables very large sections of plate to be clad in a single operation. The quality of the joint is generally good with high mechanical strength and as it is a 'cold method' the bonded metals retain their pre-bond properties. The technique has been developed with large-scale applications in the manufacturing industry for decades, and it is well known for its capability to directly join a wide variety of both similar[1–3] and dissimilar[4–7] combinations of materials that can hardly be joined by any other welding techniques.[8]

Whilst the explosive welding process is generally successful, expensive failures occur and often the causes are unknown. To improve the understanding of its physical process and mechanism, a great deal of research has been carried out,[3,9,10] but so far the results have not been satisfactory.

Different from the cases under quasi-static or low speed conditions, many important physical phenomena are accelerated under the extreme conditions during explosive welding. Diffusion is one of them and has been the focus of research.[11,12] In explosive welding, diffusion has a close relationship with the morphology of the bonding interface and the welding quality. In addition, the mechanical properties and electromagnetic properties of the weldment are affected by the diffusion layer thickness and the concentration distribution of the elements directly or indirectly. Studies of the atomic diffusion and the concentration distribution might help guide the practice of explosive welding engineering, and they might permit one to plan the direction and prospects of further studies. Experimental studies on atomic diffusion and the concentration distribution in the explosive welding processes were carried out. Akbari Mousavi and Sartangi[13] used energy dispersive spectroscopy (EDS) microanalysis and obtained the concentration distributions after the diffusion across the interface between the explosively welded cp-titanium/AISI 304 stainless steel composites. Hokamoto *et al.*[14] measured and analyzed the elemental distribution after the diffusion across the interfacial zone for metallic glass and stainless steel. In contrast, simulations on an atomic scale of diffusion and concentration distribution in the explosive welding processes have scarcely been conducted.

Molecular dynamics (MD) simulations are advantageous in revealing atomic-scale structure evolution and in interpreting the relevant experiments at the microscopic level.[15–21] Many research groups used MD simulations to study diffusion-related issues. Chen *et al.*[22] used MD simulations to investigate the effects of temperature and surface roughness on diffusion bonding in a Cu–Al system, whereas the simulations were quasi-static and there were no collisions. Delogu[23] studied the collisions between two Ni crystals with surfaces, however, the impact velocities were low and only in the range between 1 m/s and 100 m/s. Zhao *et al.*[24] showed that shock-induced melting played a key role in accelerating the initiation and propagation of self-sustained exothermic alloying reactions in Ni/Al nanolaminates, nevertheless, the relative impact velocity was 4000 m/s, which is much higher than the actual impact velocity of explosive welding, and the study did not involve diffusion. Recently, Chen *et al.*[25] reported on a study of atomic diffusion behavior in a Cu–Al explosive welding process, and demonstrated a hybrid method of calculating the diffusion layer. However, the concentration distribution of the elements across the diffusion layer was not given, and the adequacy and effectiveness of the hybrid method needs further verification.

In this study, as a continuation of our previous work,[25]

*Project supported by the National Natural Science Foundation of China (Grant Nos. 10732010, 10972010, 11332002, and 11028206).
†Corresponding author. E-mail: kliu@pku.edu.cn
© 2014 Chinese Physical Society and IOP Publishing Ltd

the welding materials are upgraded from metal–metal (Cu–Al) to alloy–metal ($Ni_{50}Ti_{50}$–Cu). The thickness of the diffusion layer is calculated by using the hybrid method. Furthermore, the concentration distribution curves of the elements are acquired and their characteristics are investigated in detail. In order to verify the results, an $Ni_{50}Ti_{50}$–Cu weldment is prepared by the explosive welding technique, and the experimental results are compared with the corresponding simulation results.

2. Method

2.1. MD simulations

Our MD simulations are performed with the LAMMPS package.[26] For all simulations, a constant integration time step of 1 fs is used. The atom interactions are described by Zhou *et al.*'s[27] alloy potentials for Ni, Ti, and Cu, in which potentials the embedded atoms method is adopted. Figure 1 shows the cell of $Ni_{50}Ti_{50}$ alloy we adopt. It belongs to the space group $P112_1/m$. The blue spheres represent Ni atoms and the grey spheres denote Ti atoms. The $Ni_{50}Ti_{50}$ alloy is martensite at room temperature and the cell is monoclinic.[28] As shown in Fig. 1(a), a, b, and c are the three sides of the cell, and $a \approx 0.288$ nm, $b \approx 0.46$ nm, and $c \approx 0.412$ nm. As shown in Fig. 1(b), the angle β between sides a and b is 96.8°.

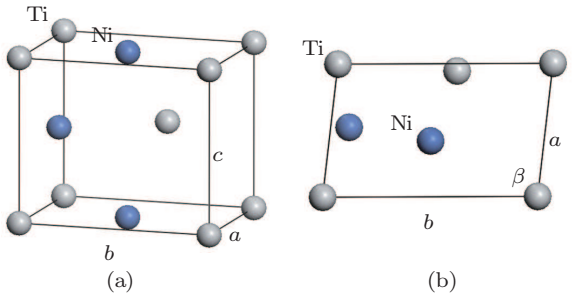


Fig. 1. (color online) Monoclinic martensitic cell of $Ni_{50}Ti_{50}$. The blue spheres represent Ni atoms and the grey spheres denote Ti atoms. (a) General view. (b) Overhead view. $\beta = 96.8°$.

The simulation process mainly contains two steps: the initialization and the collision. Figure 2 shows the configuration of the initialization. Two separated bulks, $Ni_{50}Ti_{50}$ (7.2×10^4 atoms) and Cu (7.36×10^4 atoms), are put inside a simulation box with dimensions of $2.88(x) \times 8.28(y) \times 82.2(z)$ nm^3. The length of the $Ni_{50}Ti_{50}$ bulk is 41.2 nm and the length of the Cu bulk is 36 nm. The sides a and c of the $Ni_{50}Ti_{50}$ cell are made parallel to the axes x and z, respectively. So that $10(x) \times 18(y) \times 100(z)$ $Ni_{50}Ti_{50}$ cells and $8(x) \times 23(y) \times 100(z)$ Cu cells can be exactly arranged into the two bulks, respectively. The contact surfaces of $Ni_{50}Ti_{50}$ and Cu are both (0 0 1) planes. Between them, a vacuum gap, whose length is 5 nm, is used to isolate the bulks' initial free surfaces. On both the nonimpact sides along the z axis, two transition regions which have three layers of atoms, respectively, are used to reduce the high speed shock waves' influence. Periodic boundary conditions are applied in the x, y directions. The initial thermal velocities of atoms are assumed to follow the Maxwellian distribution. With the Nose–Hoover thermostat[29] adopted, the whole system is relaxed at 293 K and zero external pressure under the constant-pressure-temperature (NPT) ensemble to finish the initialization.

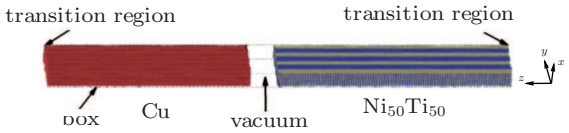


Fig. 2. (color online) The configuration of the initialization. The light blue wireframe represents the simulation box. The blue spheres represent Ni atoms and the grey spheres denote Ti atoms.

At the beginning of the following collision step, each Cu atom is given the same velocity to make the Cu bulk translate towards the $Ni_{50}Ti_{50}$ bulk, and at the same time, the transition region of $Ni_{50}Ti_{50}$ is fixed. Then the two bulks collide, while the length of the Cu bulk becomes shorter and shorter. When the Cu bulk reaches its minimum length, the transition region of Cu is fixed. Then the system is relaxed for 1000 ps under the micro-canonical (NVE) ensemble. In the end, with the final equilibrium temperature of the NVE simulation kept, the system is relaxed for another 1000 ps at zero external pressure (NPT ensemble). In brief, after the initial configuration of the model is prepared, the simulation for the welding process is divided into two stages: the loading stage and the unloading stage. This division method is consistent with the previous study focusing on explosive welding.[30] The collision velocity is set to be $u_z = -1500$ m/s and $u_x = 700$ m/s, and it is calculated according to the known explosive detonation velocity from the following equation[8]

$$V_p = 2V_d \sin(\beta/2), \tag{1}$$

where V_p is the flyer plate velocity, V_d is the detonation velocity, and β is the flyer plate dynamic bend angle.[25]

2.2. Explosive welding experiments

In order to verify the simulation results, relevant verification experiments are carried out. The basic facts about such a welding process can be found in many of the previous studies.[2–6]

Figure 3(a) presents a sketch of the initial configuration for our explosive welding technique. As shown in Fig. 3(a), the steel chopping block with a thickness of 5 cm is placed at the bottom. A $Ni_{50}Ti_{50}$ plate is laid on the chopping block serving as the base plate. Four supports stand on the $Ni_{50}Ti_{50}$ plate and support a Cu T2 plate. Supports are put on the four corners of the $Ni_{50}Ti_{50}$ plate, and they will fly off at the beginning of explosive welding. A special mixed explosive is spread on the Cu plate. The explosive is mixed with an ammonium nitrate fuel oil mixture (AN explosive) and hexogen (5%∼ 8%). The actual measured detonation velocity can reach 3800 m/s∼ 4100 m/s. An electric detonator is embedded in the left part of the explosive. By triggering the electric detonator, the explosive is detonated and drives the Cu plate to the $Ni_{50}Ti_{50}$ plate. At the colliding point, the pressure and the temperature are so high that two materials join together. In the plate collision zone, a pressure impulse occurs of about tens of GPa. Figure 3(b) presents the weldment obtained by the explosive welding technique from which we can find that the two

materials join together very well. To inspect the diffusion layer thickness of the plate-type weldment, a specimen containing the bonding interface is subjected to scanning electron microscope (SEM, HITACHI S-4800) observation (see Fig. 3(c)). The bonding interface exhibits a straight morphology.

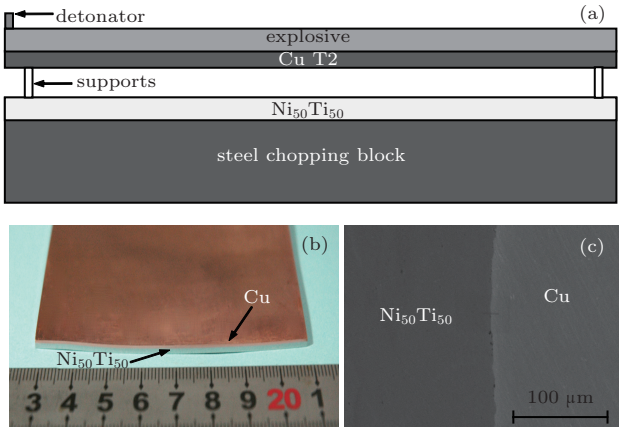


Fig. 3. (color online) (a) Sketch of the explosive welding technique. (b) Optical graph showing the $Ni_{50}Ti_{50}$–Cu weldment prepared by the explosive welding technique. (c) SEM micrograph of the interface which shows a straight morphology.

3. Results and discussion

Under the collision, the actual explosive welding process can be divided into the loading stage and the unloading stage.[30] Accordingly, our simulation for the collision is divided into two successive parts, which are mentioned above, i.e., the NVE and the NPT simulations. During the NVE simulation, i.e., the loading stage, both the temperature and the pressure experience a process that begins with a jump, goes with vibration and tends to be stable, and finally the temperature and the pressure maintain dynamic equilibrium at about 1360 K and 28 GPa respectively. In addition, no obvious diffusion is observed in this simulation, and obvious diffusion mainly takes place in the NPT simulation. The diffusivity can be described by mean-square displacement (MSD). Figure 4 shows the MSD curves obtained from the NPT simulation. As shown in Fig. 4, the MSDs of Cu and $Ni_{50}Ti_{50}$ keep increasing over time and reach about 6.1 nm^2 and 5.07 nm^2 respectively after 1000 ps. The curves approximate straight lines. It demonstrates that the system melts rapidly as soon as the system pressure has been unloaded. At the same time, Cu, Ni, and Ti atoms begin to diffuse from both sides of the interface, and the diffusivity values of Ni and Ti are a little smaller than that of Cu under the given velocity condition.

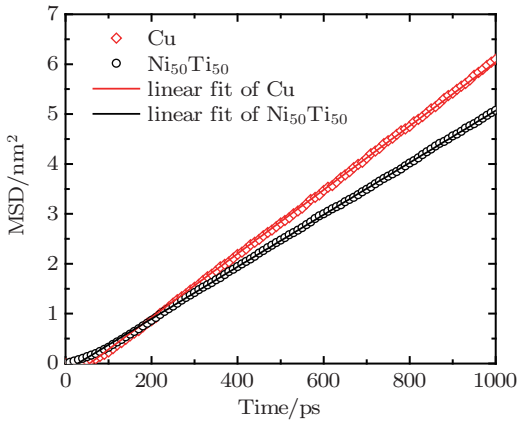


Fig. 4. (color online) MSDs versus time, obtained from the NPT simulation.

Compared with the diffusion behavior in the Cu–Al explosive welding process,[25] the diffusion behavior in the $Ni_{50}Ti_{50}$–Cu has the same conditions, similar physical processes and properties. So, a similar hybrid method can be used to calculate the thickness of the diffusion. Thus we can calculate the thickness of the diffusion layer L from the following equation[25]

$$L = \sum_{i=\mathrm{Cu,Ni_{50}Ti_{50}}} 3\sqrt{2D_i t}, \tag{2}$$

where D is the diffusion coefficient and can be calculated from the slope of the linear fitting results in Fig. 4, and t is the diffusion time and can be considered to be in the range 5 μs∼10 μs.[25,31] Therefore, we attain that the diffusion layer thickness is in the range from 1.03 μm (5 μs) to 1.45 μm (10 μs).

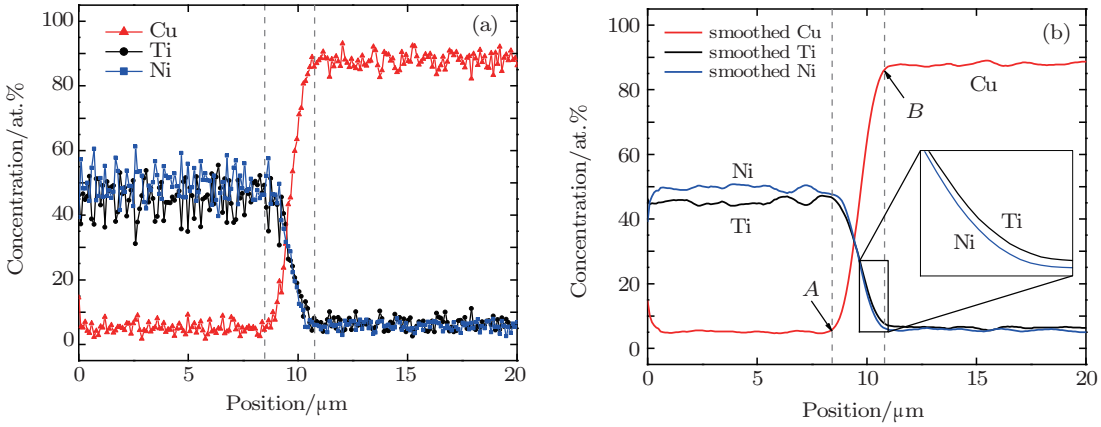


Fig. 5. (color online) (a) Atomic concentration distribution by line-scan of X-ray photoelectron spectroscopy analysis aimed at some local area at the bonding interface. The curves represent the percentages of the atom number at positions. (b) Smoothed concentration distribution curves. The dashed lines indicate the diffusion region. Points *A* and *B* are points of intersection of the dashed lines and the curves. The inset shows the local amplifications of the curves.

Figure 5 shows one of the three results of component analysis by energy dispersive spectroscopy line scanning. The scanning lines are across the bonding interface and the diffusion layer. The original experimental data are presented in Fig. 5(a) and the smoothed results are given in Fig. 5(b). The smoothing method used in this paper is called "adjacent-averaging", and the number of the adjacent points is five. The smoothed curves are all smoothed twice. The curves show the percentages of the atom number at positions along the scanning line. As shown in Fig. 5(b), the percentages of the number of Cu atoms at point *A* and point *B* are 5% and 90% respectively, and they can be roughly considered as the critical points between the diffusion layer and the non-diffusion area. Thus the width of the region between the dashed lines represents the thickness of the diffusion layer, which is about 1.98 μm. The other two energy dispersive spectroscopy results are about 1.56 μm and 2.02 μm. So the average of the three values is 1.85 μm, which is basically in line with the simulated result (1.03 μm∼1.45 μm). Given the error range of molecular dynamics simulations, the difference between the two results is acceptable. It demonstrates that the hybrid method is also effective for the calculation of ternary element explosive welding and its applicability is verified again.

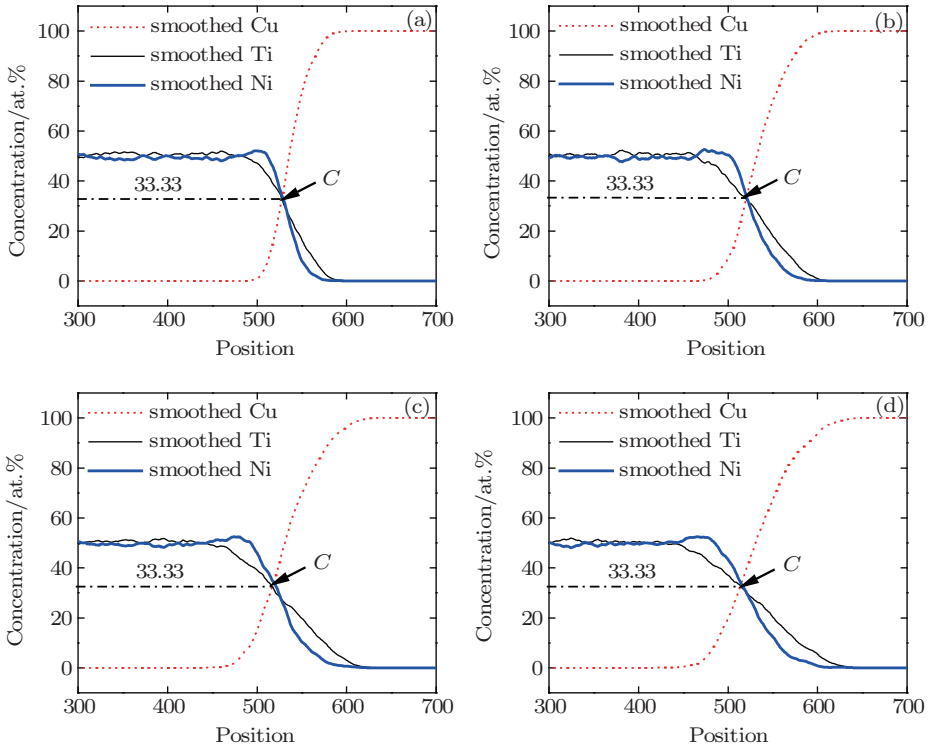


Fig. 6. (color online) Smoothed results of the atomic concentration distributions at four different times: (a) 200 ps, (b) 400 ps, (c) 600 ps, (d) 800 ps.

For a deeper understanding of the diffusion in the explosive welding process, we try to find some ways to characterize the atomic concentration distribution across the welding interface. For that reason, the simulation box is equally divided into 1000 segments along the z axis. By extracting the coordinate information of the atoms from the LAMMPS dump files, the numbers and the concentrations of the three kinds of atoms in each segment are counted and calculated, and consequently, the elemental concentration distributions at every 100 ps are obtained. Figure 6 shows the smoothed results of the concentration distributions at different simulation times. As shown in Fig. 6, the diffusivity of Ti is better than that of Ni, which is consistent with the experimental result shown in the inset of Fig. 5(b). In addition, with the time going by, the region affected by diffusion keeps expanding, and the gradients of the corresponding curves keep decreasing. However, in each graph, the shape of the curve has some characteristics in common, of which the most obvious one is that the curves almost converge to one point whose ordinate is about 33.33. The cases in the other six graphs not contained in Fig. 6 are the same. The point is denoted as *C*. In most cases, it might not be exactly on any of the three curves. One of the means to locate point *C* is to calculate the average of the abscissas of the three points, which are on the three curves respectively and whose ordinates are 33.33, and this is the means that is adopted in this paper.

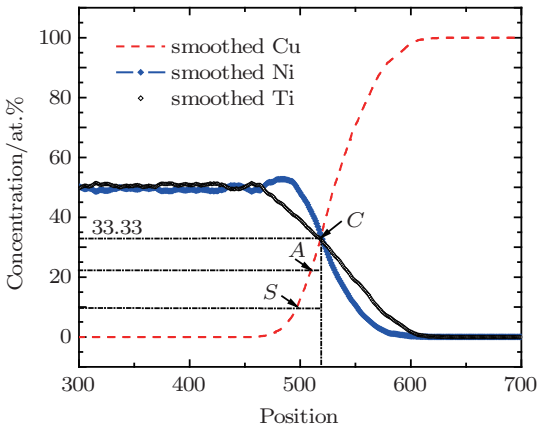


Fig. 7. (color online) Smoothed results of the atomic concentration distribution at 500 ps. Point A denotes any point on the Cu curve. Point C is the intersection point of three curves. Point S is the point on the Cu curve whose ordinate is 33.33.

Figure 7 shows the smoothed results of the atomic concentration distributions at 500 ps. In order to make quantitative analyses of the shape characteristics of the curves, variable λ is defined. For the Cu curve as shown in Fig. 7,

$$\lambda_A = \frac{\text{Position}_A - \text{Position}_C}{|\text{Position}_S - \text{Position}_C|}, \tag{3}$$

where A denotes any point on the Cu curve, C is intersection point of the three curves and S is the standard point of the Cu curve whose ordinate is 10. The definitions of λ for the Ni curve and the Ti curve are the same. λ_A represents the distance ratio and it stores the position information of the concentration which point A corresponds to.

Figure 8 shows the λ–time history of different concentrations of Cu, Ni, and Ti. The concentrations increase from 0% to 100% (Cu) or 50% (Ni and Ti) at a rate of 5%, and the time increases from 0 ps to 1000 ps at a rate of 100 ps. As shown in Fig. 8(a), with the time increasing, λ values of the concentrations from 5% to 95% can basically be considered to be unchanged, but λ values of the concentrations 0% and 100% change significantly. The former indicates that during the simulation, the concentration distribution curves of Cu keep a geometric similarity. As shown in Fig. 8(b) and Fig. 8(c), the geometric similarity can also be found in the curves of Ni and Ti. The latter is because the positions of the concentrations 0% and 100% are on the boundaries of the diffusion layer and only a few atoms can diffuse to there, and therefore the statistical results have large errors.

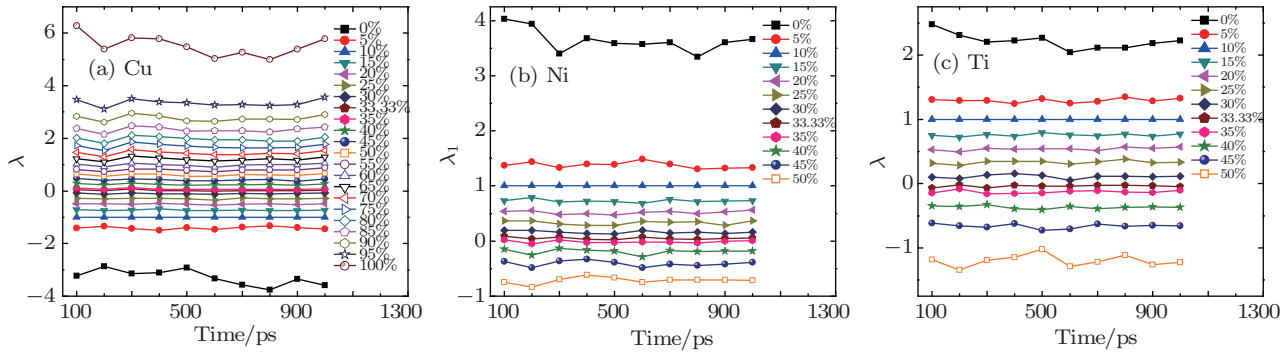


Fig. 8. (color online) λ–time history of different concentrations of Cu, Ni, and Ti, (a) Cu, (b) Ni, (c) Ti.

Figure 9 shows the comparison of λ between the simulation results and the experimental results by not considering the concentrations 0% nor 100% (Cu) nor 50% (Ni and Ti). The experimental results are calculated from the data that are also presented in Fig. 5. As shown in Fig. 9, there are few differences in both trend and values between the simulation results and the experimental results. It indicates that not only in the limited simulation time, but even for a long time in the actual explosive welding process, the geometric similarity still exists. Thus for any time in the actual explosive welding process, as long as the position or the distance information of a concentration is known, such as the thickness of the diffusion layer, the whole concentration distribution can be obtained.

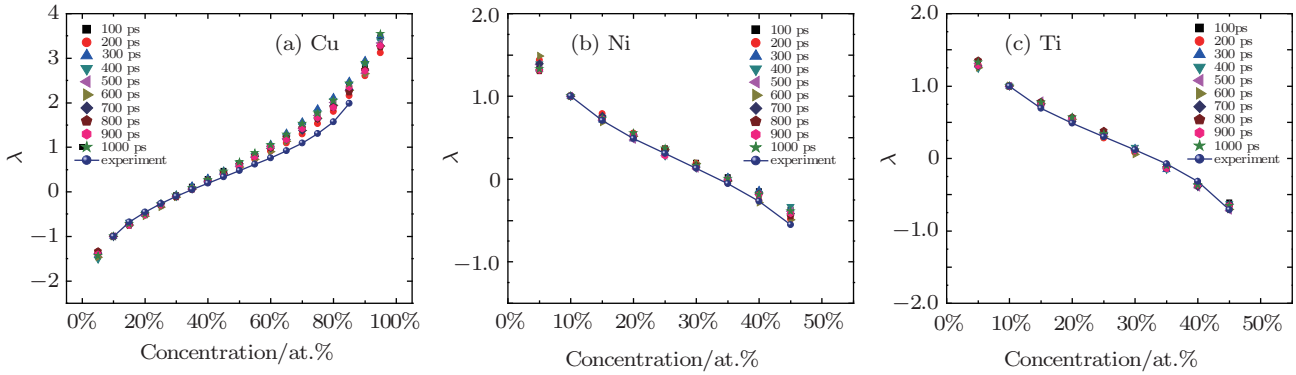


Fig. 9. (color online) Comparison of λ between the simulation results and the experimental results. The blue lines represent the experimental results and they are calculated from the EDS result shown in Fig. 5: (a) Cu, (b) Ni, (c) Ti.

Figure 10 shows the comparison of concentration distribution across the diffusion layer between the simulation results and the experimental results. The simulation results are calculated by using the geometric similarity. The position information of the 10% concentration is treated as a known value in the calculation. Obviously, the simulation results and the experimental results are in good agreement, which further proves that the geometric similarity can be described by the variable λ, and for a given concentration, λ remains unchanged during the whole diffusion process.

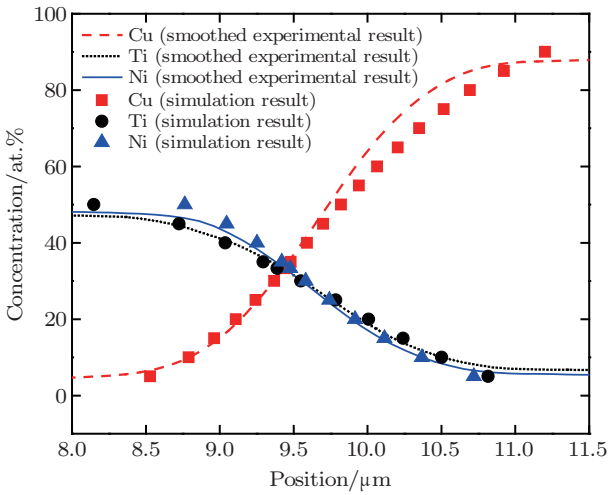


Fig. 10. (color online) Comparison of concentration distribution across the diffusion layer between the simulation results and the experimental results.

4. Conclusions

In this paper, a comparison shows that the diffusion process and properties of $Ni_{50}Ti_{50}$–Cu are similar to those of Cu–Al studied previously. The hybrid method we proposed in the Cu–Al study is used again to calculate the thickness of the diffusion layer, and the result is basically in accordance with the EDS experimental result. The application scope of the method is successfully expanded. Across the diffusion layer, the atomic concentration distributions at different times have similar geometric characteristics. The geometric similarity can be described by variable λ. For a given concentration, λ keeps unchanged in the whole diffusion process. The geometric similarity describes the shape characteristic of the diffusion layer. The calculation of the thickness of the diffusion layer describes the length characteristic of the diffusion layer. They together constitute a complete simulation procedure, which can be used to simulate the atomic concentration distribution across the diffusion layer in the actual explosive welding process.

References

[1] Kacar R and Acarer M 2004 *J. Mater. Process. Technol.* **152** 91
[2] Grignon F, Benson D, Vecchio K S and Meyers M A 2004 *Int. J. Impact. Eng.* **30** 1333
[3] Acarer M, Gulenc B and Findik F 2003 *Mater. Design* **24** 659
[4] Acarer M and Demir B 2008 *Mater. Lett.* **62** 4158
[5] Ashani J Z and Bagheri S M 2009 *Materialwiss. Werkst.* **40** 690
[6] Liu K X, Liu W D, Wang J T, Yan H H, Li X J, Huang Y J, Wei X S and Shen J 2008 *Appl. Phys. Lett.* **93** 081918
[7] Durgutlu A, Gulenc B and Findik F 2005 *Mater. Design* **26** 497
[8] Findik F 2011 *Mater. Design* **32** 1081
[9] Vaidyanathan P V and Ramanathan A 1993 *J. Mater. Process. Technol.* **38** 501
[10] Abe A 1999 *J. Mater. Process. Technol.* **85** 162
[11] Wu F M, Li Q W and Wu Z Q 2000 *Chin. Phys.* **9** 672
[12] Cao B, Li G P, Chen X M, Cho S J and Kim H 2008 *Chin. Phys. Lett.* **25** 1400
[13] Akbari Mousavi S A A and Sartangi P F 2008 *Mater. Sci. Eng. A: Struct.* **494** 329
[14] Hokamoto K, Nakata K, Mori A, Ii S, Tomoshige R, Tsuda S, Tsumura T and Inoue A 2009 *J. Alloys Compd.* **485** 817
[15] Shi Y and Falk M L 2008 *Acta Mater.* **56** 995
[16] Cao A J, Cheng Y Q and Ma E 2009 *Acta Mater.* **57** 5146
[17] Sun Y B, Luo Y, Wang X D and Feng Y Q 2011 *Adv. Mater. Res.* **217–218** 45
[18] Şopu D, Ritter Y, Gleiter H and Albe K 2011 *Phys. Rev. B* **83** 100202
[19] Shao J L, Wang P, He A M, Duan S Q and Qin C S 2013 *J. Appl. Phys.* **113** 153501
[20] Verners O, Shin Y K and van Duin A C T 2013 *J. Appl. Phys.* **114** 023501
[21] Chen Z H, Yu Z Y, Lu P F and Liu Y M 2009 *Chin. Phys. B* **18** 4591
[22] Chen S, Ke F, Zhou M and Bai Y 2007 *Acta Mater.* **55** 3169
[23] Delogu F 2010 *Phys. Rev. B* **82** 205415
[24] Zhao S, Germann T and Strachan A 2007 *Phys. Rev. B* **76** 104105
[25] Chen S Y, Wu Z W, Liu K X, Li X J, Luo N and Lu G X 2013 *J. Appl. Phys.* **113** 044901
[26] Plimpton S 1995 *J. Comput. Phys.* **117** 1
[27] Zhou X W, Johnson R A and Wadley H N G 2004 *Phys. Rev. B* **69** 144113
[28] Michal G M and Sinclair R 1981 *Acta Crystallogr. B* **37** 1803
[29] Evans D J and Holian B L H 1985 *J. Chem. Phys.* **83** 4069
[30] Wronka B 2010 *J. Mater. Sci.* **45** 3465
[31] Yan H, Qu Y and Li X 2008 *Combust. Explo. Shock+* **44** 491